AIAA JOURNAL
Vol. 40, No. 11, November 2002

Ablative Laser Propulsion: Specific Impulse and Thrust Derived from Force Measurements

Andrew V. Pakhomov,* M. Shane Thompson,† Wesley Swift Jr.,‡ and Don A. Gregory§
University of Alabama in Huntsville, Huntsville, Alabama 35899

Specific impulse, thrust, and other dynamic characteristics of solid elemental propellants for ablative laser propulsion are studied experimentally with the aid of a piezoelectric force sensor. This sensor allows direct measurements of applied thrust. Experimental results show that the highest specific impulse, ~ 4.0×10^3 s, occurs for carbon and aluminum, whereas the highest coupling coefficient (8 dyne/W) was observed for lead targets. The ablation time, derived from independent time-of-flight (TOF) experiments and used for the calculation of impulses, was ~ 1.5 μs for the majority of the elements studied. These new measurements confirm a decrease of specific impulse and an increase in thrust with increasing atomic mass of the propellant; the major trend previously determined from TOF experiments. The plasma image analysis also confirms the previously reported angular independence of ion velocity, established after the first 100 ns of plasma life. In previously reported TOF studies, all observations were based on the ionic component ejected from a laser-ablated material. An almost fivefold reduction in the absolute values of the specific impulse was observed in the current effort. This result is attributed to "dilution" of the high specific impulse values for ions by slower atomic neutrals and larger fragments. Among all of the tested elements, aluminum is found to provide the optimum tradeoff for I_{sp} and thrust values.

Nomenclature

A	=	oscillation amplitude
C_m	=	coupling coefficient
C_{mi}	=	ionic coupling coefficient
$F(t)$	=	thrust, as a function of time
I_{sp}	=	specific impulse
k	=	spring constant
m	=	mass
t	=	time
t_f	=	ablation end time
t_0	=	ablation onset time
V_0	=	value of signal decay function at $t = 0$
W	=	weight
x	=	oscillator position
γ	=	damping constant
τ_1	=	sensor waveform envelope decay time
τ_2	=	sensor waveform envelope rise time
ω	=	natural frequency of an oscillator
ω_d	=	damped frequency of an oscillator

Introduction

In an earlier paper that reintroduced ablative laser propulsion (ALP) as a viable concept,[1] Pakhomov and Gregory showed that a majority of the different schemes proposed over the years for laser propulsion have a great deal in common. (See reviews in Refs. 2 and 3 and references therein.) They employ continuous wave (cw) irradiation, leading to momentum transfer through compression waves in a laser-sustained plasma or overheated gas. Even microsecond pulses fall into this category when the timescales involved are comparable to the plasma lifetime (several microseconds); most of them used gases as propellants. In contrast to this, an ALP-based craft would be driven by high-energy, short-width (10^{-10} s and less) laser pulses, focused on a solid propellant.[1] Under such irradiation conditions, plasma formation and laser pulses are temporally separated. Therefore, instead of momentum transfer via laser-sustained detonation (or combustion) waves in the plasma, which would be dominant for longer laser pulses,[3] a momentum is imparted by direct removal, that is, ablation, of solid propellant from the target surface. We adopted the phenomenological term "ablation" as defined, for example, in Ref. 4, as a "non-thermal" phase transfer from a solid directly into a hot (10^4 K), radiant, expanding plasma. Thus, we define ablative laser propulsion as a laser-driven motion with momentum transfer dominated by direct ablation of a solid propellant.

ALP as it was just defined is strictly material dependent. The studies discussed here are directed toward practical understanding of this dependence. Our initial study concentrated on an analysis of the ablation of elementary propellants using a time-of-flight (TOF) energy analyzer. In this study, of which a detailed account is given in Ref. 5, five independent observables, ion velocity, ion yield, their corresponding angular distributions, and mass-removal rates, were analyzed. These measurements were used for the derivation of major ALP characteristics, such as specific impulse I_{sp}, momentum, energy efficiency, etc. The TOF measurements led us to four main conclusions:

1) Specific impulses, derived from ion velocities, for elementary targets ablated at irradiances of $\sim 3 \times 10^{13}$ W/cm^2 by laser pulses of 10^{-10} s width, were determined to be 2×10^4 s for carbon, 1.4×10^4 s for aluminum, and so on, down to 2.8×10^3 s for lead. In general, ion velocity and, therefore, I_{sp} are inversely proportional to the square root of the atomic mass of the ablative. Therefore, the lighter the element, the higher the specific impulse it will provide for a given irradiation condition.

2) Ion number densities are distributed proportionaly to the cosine of the angle from the normal to the target surface. Ion velocities are independent of the angle at a distance of 22 cm from the target. Thrust derived from angular distributions of ion number densities and velocities tends to increase in proportion to the atomic masses of the ablatives.

3) The lighter elements are characterized by lower mass-removal rates, whereas, for given irradiation conditions, the number of atoms removed per pulse is relatively constant. Critical exposures (i.e., the maximum number of laser pulses possible while still providing stable TOF signals) of elements are inversely proportional to their atomic masses. This observation can be explained with our preliminary discovery that critical mass (mass removed per critical

Received 29 November 2001; revision received 9 April 2002; accepted for publication 27 June 2002.

*Assistant Professor, Department of Physics. Member AIAA.
†Graduate Student, Department of Physics; currently Research Scientist, Information Systems Laboratories, Inc., Brownsboro, AL 35741. Student Member AIAA.
‡Graduate Student, Department of Physics; currently Research Scientist, Raytheon, Inc., Huntsville, AL 35812.
§Professor, Department of Physics.

exposure) is a constant for several elements for given irradiation conditions. (See Ref. 5 for details.)

4) The ionized component of the ablated material carries up to 90% of the energy delivered by the laser pulse. This indicates that ions are predominantly responsible for momentum transfer. At the same time, specific impulses derived from ion velocities set upper limits to the value of I_{sp} that can be achieved with ALP.

TOF data, based on ion velocities, allow the observation of certain trends among elemental propellants for ALP. At the same time, the unaccountability of the velocity of neutrals poses serious doubts regarding the absolute values of I_{sp} and other dynamic characteristics. Because ions comprise only a few percent of the total ablated material,[5] the inclusion of neutral components into an account of ablation dynamics has crucial importance. To clarify this issue, and to confirm (or correct) the conclusions derived from TOF experiments, we have proposed direct force measurements.[5] In this paper we present the results of these experiments. The data collected using this technique and a discussion of some difficulties encountered in the course of the measurements will also be described.

Experimental Technique

The experimental setup is presented in Fig. 1. The laser system, 1, comprises a seeding laser (mode-locked Coherent Antares) and a regenerative amplifier (Continuum RGA60). The laser system was tuned to the second harmonic output (532-nm wavelength), and it generated single or repetitively (up to 10 Hz) emitted pulses of width ~100 ps and energy ~8 mJ at the target. Selection of the output pulse from the amplified train was monitored by a LeCroy 9450 Digital Storage Oscilloscope, whereas pulse energy was measured by a broadband energy/power meter (Melles–Griot 13PEM001). The laser pulse from the laser system was redirected by a system of folding mirrors, 2, onto a vertical arrangement composed of a focusing lens, 3; an optical window, 4; and a sample, 5. The sample was placed horizontally on top of the piezoelectric force sensor, 6 (PCB Piezotronics, Model 209C01), which has a resolution 10^{-4} N. A plano-convex lens, 3, of focal length 20 cm was used to provide an irradiance of $\sim 6 \times 10^{12}$ W/cm^2, near the diffraction limit, focused on the target of $\sim 6 \times 10^{12}$ W/cm^2. The optical window, 4, was attached to the ablation chamber, 7, at Brewster's angle to minimize reflection losses. The force measurements were performed in air at atmospheric pressure. When needed (see hereafter) the ablation chamber was maintained at a vacuum of $\sim 3 \times 10^{-3}$ torr by the pumping system, comprising a roughing pump (Alcatel 2002 BB) and a diffusion pump (Varian HS-2). The pressure was measured by a thermocouple gauge (Kurt Lesker KJL-6000), attached approximately 40 cm downstream from the sample. The pressure readings from the gauge were taken with the controller (Kurt Lesker IG4400).

The piezo sensor was connected via a vacuum feedthrough to a signal conditioner, 8 (PCB Piezotronics Model 482B06), which passed amplified signals to a digital oscilloscope, 9 (Tektronix TDS 460A). The oscilloscope was triggered by a fast photodiode, 10 (Thorlabs DET210, rise time 1.0 ns), positioned near the optical window, 4. The signal from the sensor was recorded by the oscilloscope, 9, and then analyzed with a personal computer, 11, using a set of programs written in Mathematica (version 4.0).

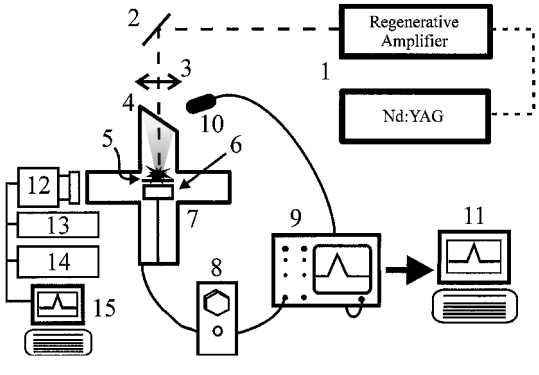

Fig. 1 Experimental setup.

In parallel with the force measurements, time-gated imaging of plasma plumes was performed. (In this case measurements were conducted in vacuum as well as in air.) This auxiliary setup included an intensified charge-coupled device (CCD) camera, 12, Model ICCD576C/1THX, a PG-200 programmable pulse generator, 13, and an ST 130 detector controller, 14, all made by Princeton Instruments. The pulse generator was triggered by the photodiode, 10, on arrival of the laser pulse. The images of the plasma were analyzed on a personal computer, 15, using a set of programs written in Interactive Data Language (IDL) version 3.5. The system allowed the imaging of the laser-induced plasma at the rate of a single frame per laser shot. The minimum allowable time delay was 18 ns, the gating speed of the system was 2.0 ns, and the spatial resolution was 75 μm. The shot-to-shot images for each delay time were virtually identical.

A set of flat elemental targets representing a reasonably broad range of atomic masses was chosen: carbon (graphite), aluminum, iron, copper, zinc, tin, and lead. These targets had masses in the range 80–350 mg, that is, the target masses were much smaller compared to those used in Ref. 5. Mass-removal rates were determined by simply weighing the sample before and after exposure. Because of the minute masses removed per shot, an accumulation of removed mass was achieved by using multiple exposures. The detrimental effects due to crater formation were obviated in the same manner as described in Ref. 5, that is, the number of shots per fixed target position was kept less than the critical exposure. (See the definition in the Introduction.)

Results and Discussion

Plasma Imaging

Plasma plume imaging by the intensified CCD (ICCD) camera had several objectives. First, we expected to measure plume expansion velocity and compare it to the ion velocity measurements derived from previous TOF experiments.[5] Second, in anticipation that the time of ablation can actually be shorter than the rise time of the force sensor (5 μs), we realized that an improved method would be needed to measure the plasma for an estimation of imparted momentum more accurately.

A typical plasma plume created using a lead sample at 500-ns and 1-μs delays in vacuo is presented in Fig. 2. The dimensions and position of the sample are indicated in Fig. 2. As one can see, the plasma plume has an elongated shape along the normal to the sample surface, and it exhibits clear azimuthal symmetry, which we used in the derivations of ion yield and imparted momentum in Ref. 5. This sort of plasma image was used for the derivation of plasma plume contours. The plume edge was defined at 10% of maximum intensity. The initial choice of the 10% criterion came from the standard definition of the rise time in photodetectors.[6] However, further analysis of plasma images revealed that 10% of maximum intensity criterion also provided the best shot-to-shot reproducibility of plasma edge contours, which was generally better than 3%. The plume images were taken from consecutive laser shots at a fixed delay (>250 ns) and exposure times. Examples of such edge contours are presented in Fig. 3. The lead plasma profiles shown here are typical of the observation for all tested materials. The distortion of plume shapes seen in Figs. 2 and 3 is likely due to scattered light from the walls of the ablation chamber.

The expansion velocity along the surface normal, derived from these contours, is 12.5 km/s, which is about one-half the value reported using TOF measurements with lead.[5] This difference can be explained by the following considerations. The actual pulse energy delivered to the target in these measurements was 8 mJ. The reduction of pulse energy was due to losses along the optical path in the experimental setup. (The actual folded system was composed of more than a single mirror, as schematically shown in Fig. 1.) Note that 8 mJ is ~ one-quarter of the pulse energy used for ablation in the TOF system. Assuming the same energy efficiency for both schemes, one must anticipate that the ratio of ion velocities will be proportional to the square root of the energy ratio. In this case, it should be about $1/\sqrt{4}$, and this is what we have observed. To check our understanding, we have performed TOF measurements on all elements at reduced (8 mJ) pulse energy. (See Ref. 5 for experimental

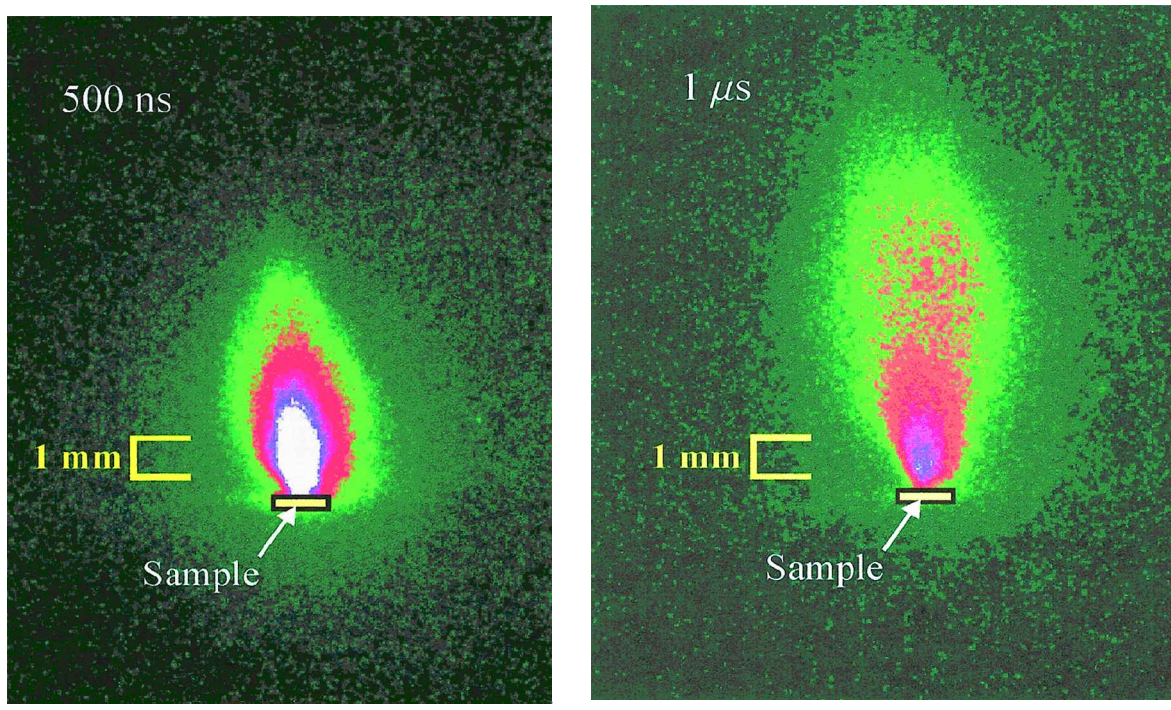

Fig. 2 Plasma plumes observed on lead target (exposure time 20 ns) in vacuo; delay times are a) 500 ns and b) 1 μs.

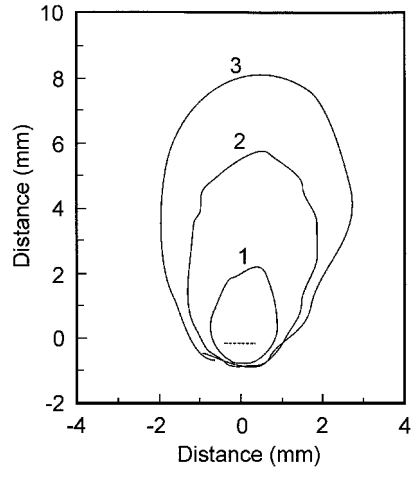

Fig. 3 Edge contours of plasma plume observed with lead target (exposure time 5 ns); delay times are 1, 500 ns; 2, 750 ns; and 3, 1 μs; - - - -, position of the sample.

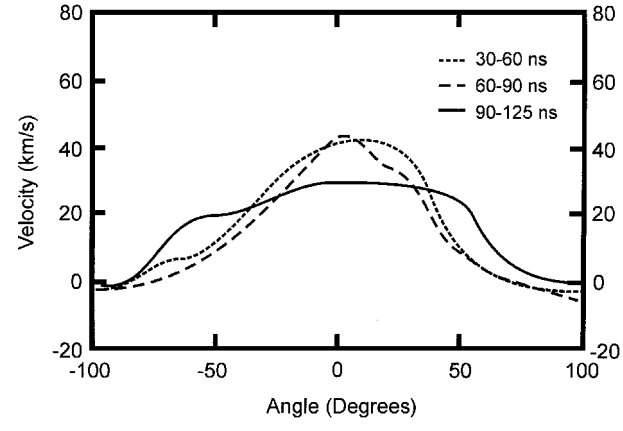

Fig. 4 Angular velocity distributions derived from plasma plume contours for aluminum target. (Delay times used for velocity derivation are indicated.)

details.) All elements exhibited similar twofold reduction of ion velocity.

Of course, one should exercise certain caution in velocity estimation from temporally resolved plasma contours. The intensity contour is not yet a pure marker for the propagation of plasma constituents, mostly because the measured intensity is a function of time on its own. However, such a simplified approach appears useful, for example, as a less expensive alternative to the ICCD technique for conversion of spatial resolution of plasma plumes into temporal resolution.[7] Profiles derived from plasma images using IDL are presented in Fig. 4 (aluminum target). As the delay time increases, the profile tends to change its form from an initially bell-shaped sharp feature to a flat, equilibrated velocity distribution at a later time. Thus, according to the data of Fig. 4, equilibrium is established after the first 100 ns, within a 100-deg angular span. This result strongly corroborates earlier observations (with the TOF experiments) of the directional independence of ion velocity[5] at large distances from the target (22 and 42 cm), corresponding to much later times (~10–20 μs). This initial finding definitely encourages further study. At this point, some features remain unclear. For example, the velocity profile corresponding to 30–60 ns time delays looks sharper than that corresponding to the 60–90 ns time delay. One of the possible reasons is a much stronger noise signal at earlier delay times, when the plume is naturally the smallest. Further studies of plasma velocity profiles with actual three-dimensional imaging and, ultimately, the modeling of electron densities as a function of spatial coordinates and time, are underway.

Ablation Time

Another quantity derived from plasma imaging was the duration of the ablation, that is, the time interval (t_0, t_f) in the equation defining the specific impulse:

$$I_{sp} \equiv \frac{1}{W} \int_{t_0}^{t_f} F(t)\, dt \tag{1}$$

where W is the weight of the ablated propellant. [See further discussion of Eq. (1) and its implications to ALP in Ref. 5.]

Assuming that ablation occurs as long as one can detect an intensely glowing plasma plume, the ablation was steadily observed for 1–1.5 μs for all targets. At longer delays, the intensity of the

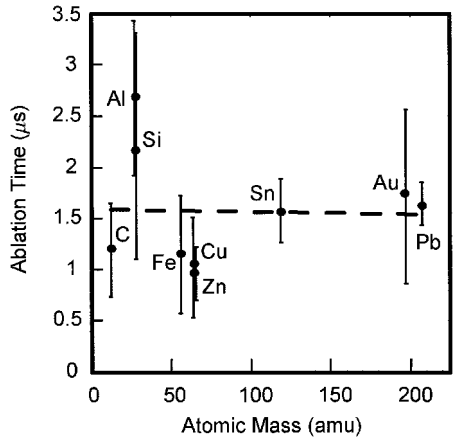

Fig. 5 Ablation times of tested elements (- - - -, numerical fit).

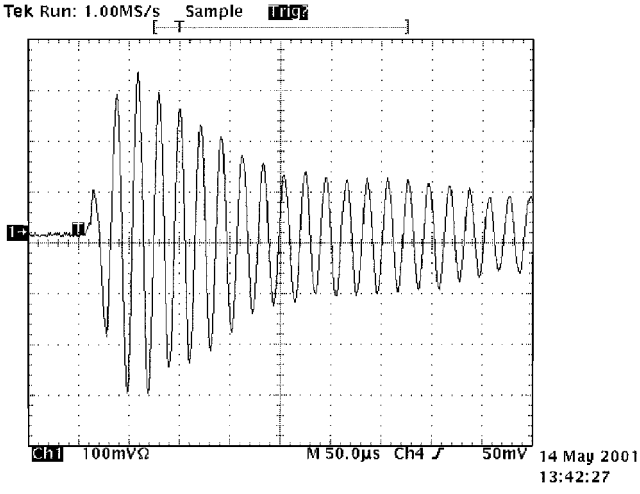

Fig. 6 Typical waveform from force sensor (Sn target).

radiation was equal to or less than 1% of the intensity maximum. Also, we have been able to observe actual detachment of the plasma plume from the surface of the target at ~1-μs and longer delays. These observations were collected frame by frame with a 50-ns interval and were combined into a brief, colorful animation. Shareware Ulead Gif Animator 5.0 was used for this purpose. In addition to the colorful appearance, these observations posed a challenge to our measurements: the ablation times were shorter than the rise time of our piezoelectric sensor (5 μs). To determine I_{sp} using Eq. (1), we needed an independent way to measure the time interval (t_0, t_f).

From available experimental data, the best presentation of the ablation time is given by the temporal width of the TOF waveforms, corresponding to the time of charge deposition. We first determined full-widths at half-maximum (FWHM) measured at a reduced pulse energy of 8 mJ. Then we extrapolated the FWHM to the zero distance from the target. (This technique was suggested in Ref. 8.) The FWHM of the TOF waveform form a straight line when plotted on a logarithmic scale as a function of distance from the target. This follows from FWHM increasing exponentially with time. The actual ablation time was derived from FWHM by fitting the waveforms to the power function, with an error of less than 0.5%. The results of these extrapolations are presented in Fig. 5. Atomic mass was used as the abscissa (x coordinate) of Fig. 5 purely for presentation purposes. There is no dependence on atomic mass, as illustrated by the practically flat fitting line, corresponding to the 1.5-μs mean. This result agrees reasonably well with the time of the observed cessation of plasma plumes. The ablation times presented in Fig. 5 were used for estimation of the impulse imparted to the targets.

Force Measurements

A typical oscilloscope waveform taken from the piezoelectric sensor (on the laser pulse arrival) is presented in Fig. 6. (The Sn sample was used in this example.) The signal is composed of resonant 100-kHz oscillations modulated by the system rise and decay times. The Fourier transform of the waveform is presented as an insert in Fig. 7, where the carrier frequency of an oscillator can be clearly seen. As stated earlier, the rise time of the sensor (5 μs) exceeded the ablation time, that is, the time interval over which the force is actually applied to the target. Therefore, we had to retrieve the values of the force imparted to the targets by an extrapolation of the force to shorter times. To do this, an algorithm was developed consisting of the following steps:

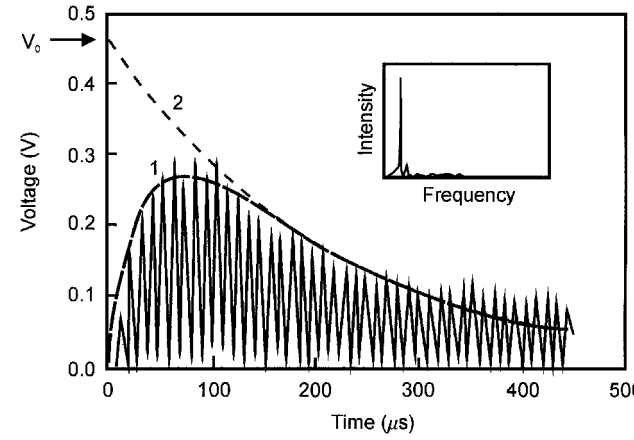

Fig. 7 Transformed waveform with numerical fit and extrapolation (see comments in the text); insert shows Fourier transform of an actual waveform.

1) Each waveform was represented by 500 digitized time/output voltage data pairs at 1-μs intervals starting about 50 data points before the arrival of the laser pulse, occurring at the time $t = 0$. The mean value of the signal before $t = 0$ was subtracted from the signal to compensate for system offset drift.

2) The absolute value of the signal after $t = 0$ was taken, and the crests of the waveform were marked to define the envelope of the signal. (See curve 1 of Fig. 7.) The waveform transformed by this operation is given in Fig. 7. The instrument response function $F(t)$ is represented by an exponential rise and decay of the waveform envelope. Equation (2) was fitted to curve 1 using a least-squares technique:

$$F(t) = V_0 \exp(-t/\tau_1)[1 - \exp(-t/\tau_2)] \tag{2}$$

where τ_1 and τ_2 represent the best-fit decay and rise time constants, respectively, and V_0 is the sensor voltage at $t = 0$, that is, the actual thrust that we need to estimate. V_0, in volts, was converted into Newtons using a sensor calibration constant. The sensor has a manufacturer-certified calibration constant of 494,604 mV/kN, which held over the dynamic range 10^{-4}–10 N.

3) The impulse was estimated by the area of a triangle with a base equal to the ablation time of the given element and a height V_0. Specific impulse was derived by dividing the impulse by the weight of the ablative material removed per shot [Eq. (1)].

The force measurements were based on the extrapolation described earlier. The time constants τ_1 and τ_2 revealed quite high reproducibility over all varieties of samples studied thus far. The rise time constant was $\tau_2 = (10 \pm 3)$ μs on the whole set of various elementary targets, whereas shot-to-shot reproducibility for the same target was better than 2%. This value reasonably exceeds the rise time for the unloaded sensor (5 μs), which can be viewed as a lower bound for τ_2. The additional 2–8 μs of τ_2 above the sensor rise time are presumably due to the path the signal takes to the oscilloscope through the signal conditioner (see Fig. 1). The variation of the rise time from sample to sample we tend to attribute to the difference in the sample–sensor mechanical coupling, that is, the actual geometry involved in positioning the sample on the sensor. All of our efforts to induce a change in the rise time, by changing sample mass, placing a viscous fluid (vacuum grease) between the sample and the sensor, using longer cables between signal conditioner and oscilloscope, have not revealed any trend affecting τ_2.

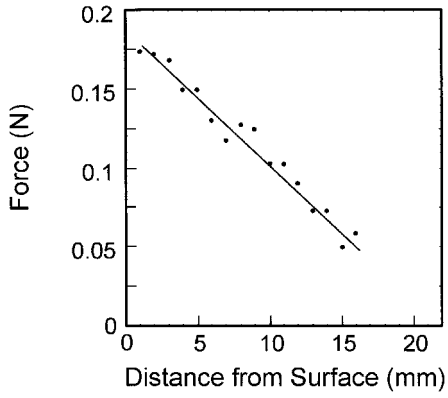

Fig. 8 Force measured for a focusing lens moved away from the target (Pb), placed initially at the focus; ——, the trend in the data.

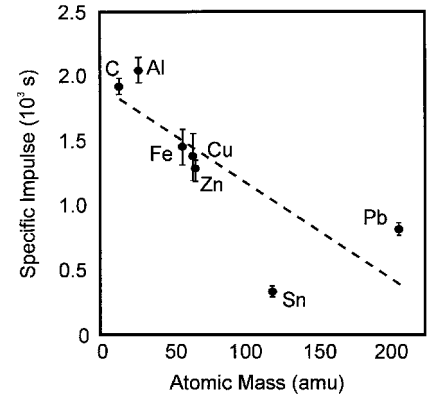

Fig. 9 Specific impulse vs atomic mass of propellant derived from force measurements; - - -, the trend in the data.

The decay time τ_1, used for extrapolations to $t = 0$, demonstrated a spread of values similar to that for τ_2: (203 ± 74) μs over all samples and the same shot-to-shot reproducibility. The decay time was used in a simple mechanical analog of mass–spring model, represented by a one-dimensional equation of motion of a damped oscillator:

$$\ddot{x} + 2\gamma\dot{x} + \omega^2 x = 0 \tag{3}$$

where ω is the binding frequency of the oscillator and x is its position. The reciprocal of the decay time is found from the fit determined with γ. The natural frequency $\omega = \sqrt{(k/m)}$. The solution of Eq. (3) is the function

$$x(t) = A\exp(-\gamma t)\sin(\varpi_d t + \phi) = A\exp(-\gamma t)\cos(\varpi_d t) \tag{4}$$

where A is the amplitude, ω_d is the damped frequency and ϕ is the phase angle. If it is further assumed that the force is applied at $t = 0$, giving maximum compression, the phase angle is $\pi/2$, and the solution is simplified to the second expression in Eq. (4). Using this mechanical model, we were able to fit experimental data with an accuracy of $\sim$1%.

As stated earlier, the force measurements were performed in air. This was due to the construction of the sensor, which did not allow vacuum measurements. The piezoelectric crystal compartment is sealed in nitrogen at 1-atm pressure. One of our concerns was the effect of the atmosphere on our measurements and, in particular, the possible addition of pressure from the shock wave induced in the air breakdown. To address this problem, we performed force measurements during the gradual removal of a focusing lens away from the sample. If air pressure made a significant contribution to the force measurement, we expected to observe an inverse square (distance) dependence on the force, due to the approximately spherical symmetry of the air breakdown. Also, for air effects, one can expect an independence of force measurements from target material. This type of behavior has actually been observed for longer pulses, as discussed, for example, in Ref. 9.

Neither of these expectations materialized. The force decreased linearly with the distance. An example is given in Fig. 8. The data were taken using a lead sample. Presumably, the reason for such behavior is a gradual partitioning of the pulse energy between the breakdown at the target surface and the air. The latter portion increases with distance. At longer distances, two separate breakdowns are clearly observed.

Specific Impulse and Thrust

The specific impulses, derived using the algorithm described earlier, are presented in Fig. 9. Error bars in Fig. 9 were inferred from the data scatter and represent one standard deviation.

When these results are compared to the conclusions in Ref. 5, it can be seen that the inclusion of neutral components in I_{sp} makes it no longer inversely proportional to the square root of atomic mass. However, the trend in the data is still the same: Lighter elements provide higher I_{sp}. More important, as expected, the absolute values of I_{sp} are about one order of magnitude lower than those derived from

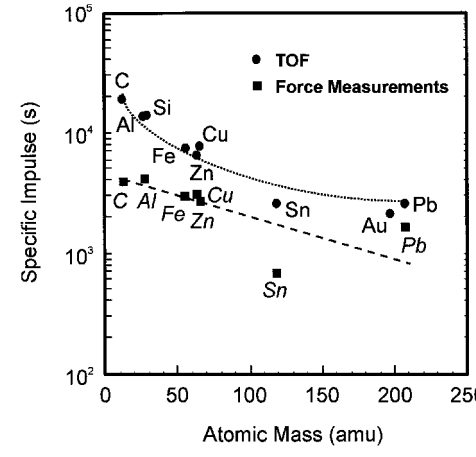

Fig. 10 Specific impulse vs atomic mass of propellant as derived from TOF experiments (Ref. 5; ●) and force measurements, ■; - - - - and - - -, numerical fit.

ion velocities in Ref. 5. This difference can only partly be attributed to the difference in laser pulse energy, which, as discussed in the preceding section, leads to a twofold reduction of ejecta velocity. In other words, the direct comparison of data from Ref. 5 and this work would require the data of Fig. 9 to be multiplied by a factor of two. Figure 10 presents such a comparison with corresponding correction for the pulse energy. In a sense, Fig. 10 shows the upper bound for I_{sp} within given irradiation conditions, in the ideal case where the ionization is 100%. Of course, the reduced actual I_{sp} comes from accounting for removed neutrals, as discussed hereafter.

As one can see from Figs. 9 and 10, the lightest elements (Al and C) provide the highest specific impulse, which confirms previous observations based on TOF analysis.[5] Note that our I_{sp} data for aluminum match well the 4900 s measured by researchers at the Massachusetts Institute of Technology Lincoln Laboratory (as communicated by D. A. Gonzales in October 2001), who employed piezoelectric disk benders as a force sensor and 500-ps pulses from a miniature Nd:YAG laser of their own invention for generating the thrust.[10]

The data in Fig. 9 are based on three independently measured quantities: ablation time, force, and removed mass. The mass-removal rates used for the derivation of I_{sp} are presented in Fig. 11. The rates were generally lower than those reported in Ref. 5: Their absolute values were shifted from micrograms into the hundred-nanogram range. This could be due to the pulse energy difference, which was 8 mJ in these experiments, one-quarter of the pulse energy in Ref. 5. However, the rates did demonstrate the same trend vs the atomic mass of the propellant, as shown in Fig. 11. The reduced pulse energy made already laborious mass-removal measurements almost impractical due to a combination of two mutually exclusive conditions: accumulation of a large number of shots and the need for a fresh sample surface per shot to not exceed the critical

Table 1 Coupling coefficients

Element						
Carbon	Aluminum	Iron	Copper	Zinc	Tin	Lead
		C_m, dyne/W				
2.6	4.3	4.6	2.7	5.6	3.5	8.0
		C_{mi}, dyne/W				
0.4	0.8	1.15	1.2	1.55	1.1	2.0

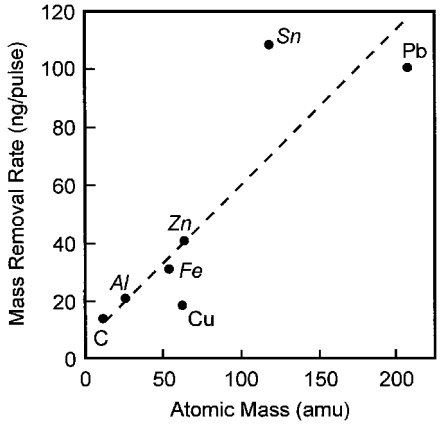

Fig. 11 Mass-removal rates vs atomic mass of propellant: – – –, the data trend; for elements denoted in italics, the data were interpolated from Ref. 5.

exposure. Thus, actual removals were determined only for carbon, copper, and lead (two extrema and one median point from Fig. 11). For other elements, the rates were found via linear interpolation of mass-removal rates assessed for all of the elements studied at higher pulse energies (30 mJ). These data were presented in Ref. 5. Comparing mass-removal rates in air and in vacuum, we found that the mass removal in air was about one-half that in vacuum, which is most likely due to enhanced (by air pressure) redeposition of ablatives. (See, for example, Ref. 11.) To be consistent with our reported force measurements, performed in air, we used in-air mass-removal rates to determine the I_{sp} values given in Figs. 9 and 10.

The coupling coefficients C_m derived from force measurements are presented in Table 1. We defined C_m as the momentum imparted to the target by ablation divided by the laser pulse energy, which is traditionally measured in mixed notation of dynes per watt. Table 1 demonstrates a similar trend, in thrust as a function of atomic mass, to that presented in Ref. 5. Lead is the leader in this category, whereas the lightest, carbon, is rather close to the end of the list. The result for lead deserves special noting, because about half the ablated mass is removed during a phase explosion (PE), which follows the initial plasma burst with a regular 50-μs delay. (Similar effects were observed with tin.[12]) Compared to the initial laser-induced plasma, the velocity of fragments removed via phase explosion is ~100 times less, and, therefore, in terms of imparted momentum, the PE constitutes a pure loss. Returning to the data of Table 1, aluminum exhibited high thrust and, at the same time, had the best I_{sp} (Fig. 9). This places aluminum in the list of primary candidates for future ALP studies. In general, the absolute values of the coupling coefficients reported here are in the upper tier of C_m reported by other researchers investigating laser ablation for propulsion (for example, Ref. 13).

Now, with the coupling coefficients obtained from direct force measurements, we can compare them to those derived from TOF data.[5] For this purpose, we may define the ionic coupling coefficient C_{mi} as a product of the number of all ions removed per shot, divided by the laser pulse energy. Thus, the normalization of the imparted momentum over the laser pulse energy allows us to compare the results of TOF measurements with direct force measurements, in spite of the difference in pulse energies. As an example, consider lead, where C_{mi} was 2.0 dyne/W. The mass of those ions was just 1.5% of all removed mass, whereas C_{mi} is just four times less than the corresponding C_m value (8.0 dyne/W). A similar relationship can be obtained for other metals (Table 1). Keeping in mind that C_{mi} values were derived from measured TOF waveforms, taken 22 cm away from the target, we can account for the difference between C_{mi} and C_m and attribute it to the loss of ion number density (recombination, scattering) occurring over this distance. Thus, the correspondence between C_{mi} and C_m likely indicates that the thrust, as I_{sp}, is primarily determined by an ionic component of the plume.

The fact that ions, representing the mass-carrying component of laser-induced plasma, define the dynamics of ablative momentum transfer should not be surprising. However, the numerical assessment of mechanical characteristics, such as the specific impulse and thrust, still requires consideration of neutral components present. One of the general conclusions drawn from our experiments is that the role of neutral components in ablative momentum transfer can be limited to accounting for lost mass. The momentum transfer of neutrals is negligible.

Conclusions

A combination of measurements involving plasma plumes, a piezoelectric-based direct force measurement, and data from earlier TOF ion velocity measurements lead us to four main conclusions:

1) Specific impulse derived from direct force measurements on elementary targets is about five times less than those reported from TOF measurements. The general trend reported from the TOF study is still the same: The lighter the element, the higher the specific impulse it will provide for given irradiation conditions. The highest I_{sp} is achieved with aluminum and carbon targets (2×10^3 s).

2) Thrusts tend to increase proportionally to the atomic masses of the ablatives, that is, they exhibit the same trend as the one derived from TOF experiments. Although lead provides the highest thrust, aluminum targets show the best tradeoff between thrust and I_{sp}. Coupling coefficients derived from direct force measurements are in the range of 2–8 dyne/W.

3) Ion velocities derived from plasma imaging match previous TOF measurements well. Determined from TOF experiments, the angular invariance of the ion velocity was confirmed by plasma imaging. Equilibrium is established after ~100 ns. Ablation times derived from plasma imaging and TOF waveforms are ~1.5 μs.

4) The ion component is the main provider of momentum transfer for ALP. Therefore, in assessing the dynamic characteristics for ALP, the role of neutral components primarily accounts for mass losses.

Analysis of data from the experiments presented in this investigation allows a much more accurate determination of the specific impulse generated by the ablation process than any single parameter measurement taken alone. Of the materials tested, aluminum and carbon were found to exhibit the highest specific impulse (2.0×10^3 s), whereas the highest thrust was achieved for lead targets. Among the tested elements, aluminum was found to provide an optimum tradeoff between I_{sp} and thrust values. Major trends previously reported for ALP from TOF experiments, such as a decrease in specific impulse and an increase in thrust with increasing atomic mass of the propellant, are confirmed by our analysis of force data.

Acknowledgments

This work was performed in conjunction with Information Systems Laboratories (ISL), Inc. (Brownsboro, Alabama, branch), under NASA Small Business Technology Transfer Grant NAS8-00185. Additional resources were also provided by the National Science Foundation Research Experience for Undergraduates Grant ATM9820339 and the University of Alabama in Huntsville Mini-Grant Research Program. The help of James D. Brasher and Thomas W. Johns of ISL, Inc., is greatly appreciated.

References

[1]Pakhomov, A. V., and Gregory, D. A., "Ablative Laser Propulsion: An Old Concept Revisited," *AIAA Journal*, Vol. 38, No. 4, 2000, pp. 725–727.

[2]Caveny, L. H. (ed.), *Orbit-Raising and Maneuvering Propulsion: Research Status and Needs*, Progress in Astronautics and Aeronautics, AIAA, New York, 1984, pp. 1–200.

[3]Glumb, R. J., and Krier, H., "Concepts and Status of Laser-Supported Rocket Propulsion," *Journal of Spacecraft and Rockets*, Vol. 21, No. 1, 1984, pp. 70–79.

[4]Russo, R. E., "Laser Ablation," *Applied Spectroscopy*, Vol. 49, No. 9, 1995, pp. 14A–28A.

[5]Pakhomov, A. V., Thompson, M. S., and Gregory, D. A., "Specific Impulse and Other Characteristics of Elementary Propellants for Ablative Laser Propulsion," *AIAA Journal*, Vol. 40, No. 5, 2002, pp. 947–952.

[6]*The Photonics Dictionary*, 45th ed., Laurin, Pittsfield, MA, 1999, p. D-122.

[7]Bulatov, V., Krasniker, R., and Schechter, I., "Converting Spatial to Pseudotemporal Resolution in Laser Plasma Analysis by Simultaneous Multifiber Spectroscopy," *Analytical Chemistry*, Vol. 72, No. 13, 2000, pp. 2987–2994.

[8]Fajardo, M. E., "Velocity Selection of Fast Laser Ablated Metal Atoms by a Novel Nonmechanical Technique: Temporally and Spatially Specific Photoionization (TASSPI)," U.S. Air Force Research Lab., AFRL Final Rept. PL-TR-97-3051, Edwards AFB, CA, Feb. 1998.

[9]Hettche, L. R., Tucker, T. R., Schriempf, J. T., Stegman, R. L., and Metz, S. A., "Mechanical Response and Thermal Coupling of Metallic Targets to High-Intensity 1.06-μ Laser Radiation," *Journal of Applied Physics*, Vol. 47, No. 4, 1976, pp. 1416–1421.

[10]Gonzales, D. A., and Baker, R. P., "Microchip Laser Propulsion for Small Satellites," AIAA Paper 2001-3789, July 2001.

[11]Preuss, S., Demchuk, A., and Stuke, M., "Sub-Picosecond UV Laser Ablation of Metals," *Applied Physics A*, Vol. 61, No. 1, pp. 33–37.

[12]Pakhomov, A. V., Thompson, M. S., and Gregory, D. A., "Phase Explosion in Elementary Targets Exposed to Picosecond Laser Irradiation," *Journal of Applied Physics* (submitted for publication).

[13]Phipps, C. R., Luke, J., and Marquis, J., "Diode Laser-Based Microthrusters: A New Departure in High I_{sp}, Long-Life Engines," AIAA Paper 2000-3477, Aug. 2000.

M. Sichel
Associate Editor